

Introduction to motion of charged particles in Earth's magnetosphere

Yuting Ng

University of Illinois at Urbana-Champaign

Masahiro Hoshino, Takanobu Amano, Keisuke Shirakawa, Katsuaki Higashimori

The University of Tokyo, Graduate School of Science, Department of Earth and Planetary Science, Masahiro Hoshino Laboratory

This report presents a brief and simple introduction to the motion of charged particles in the Earth's magnetosphere. Separated into three parts, the first portion goes over the structure of the magnetosphere, including plasma regions, field morphology and general modeling schemes. The second section addresses the simulation of relativistic charged-particle trajectories such as the governing equations of motion and the available motion solvers. Finally, the last component of this article discusses the projects, exploring wave-particle resonances, undertaken during the UTRIP 2013 summer research program.

Introduction

Energetic particles trapped in the Earth's magnetosphere affect our daily lives in many ways. Due to their high energies, they are potentially damaging to space equipment such as GPS and communication satellites. Fields and currents set up by the motion of these particles are felt on ground power lines, causing possible disruptions in power supply. Radiation from such particles also pose health hazards to aircraft personnel and passengers. On the other hand, the interactions of these energetic particles with the Earth's ionosphere lead to dazzling aurora displays. In addition, these particles are also be found in outer space. Results from studies of these particles in the Sun-Earth system might be applied to explain other astrophysical phenomena. Thus, understanding the source and subsequent transportation of such particles is of practical and scientific importance.

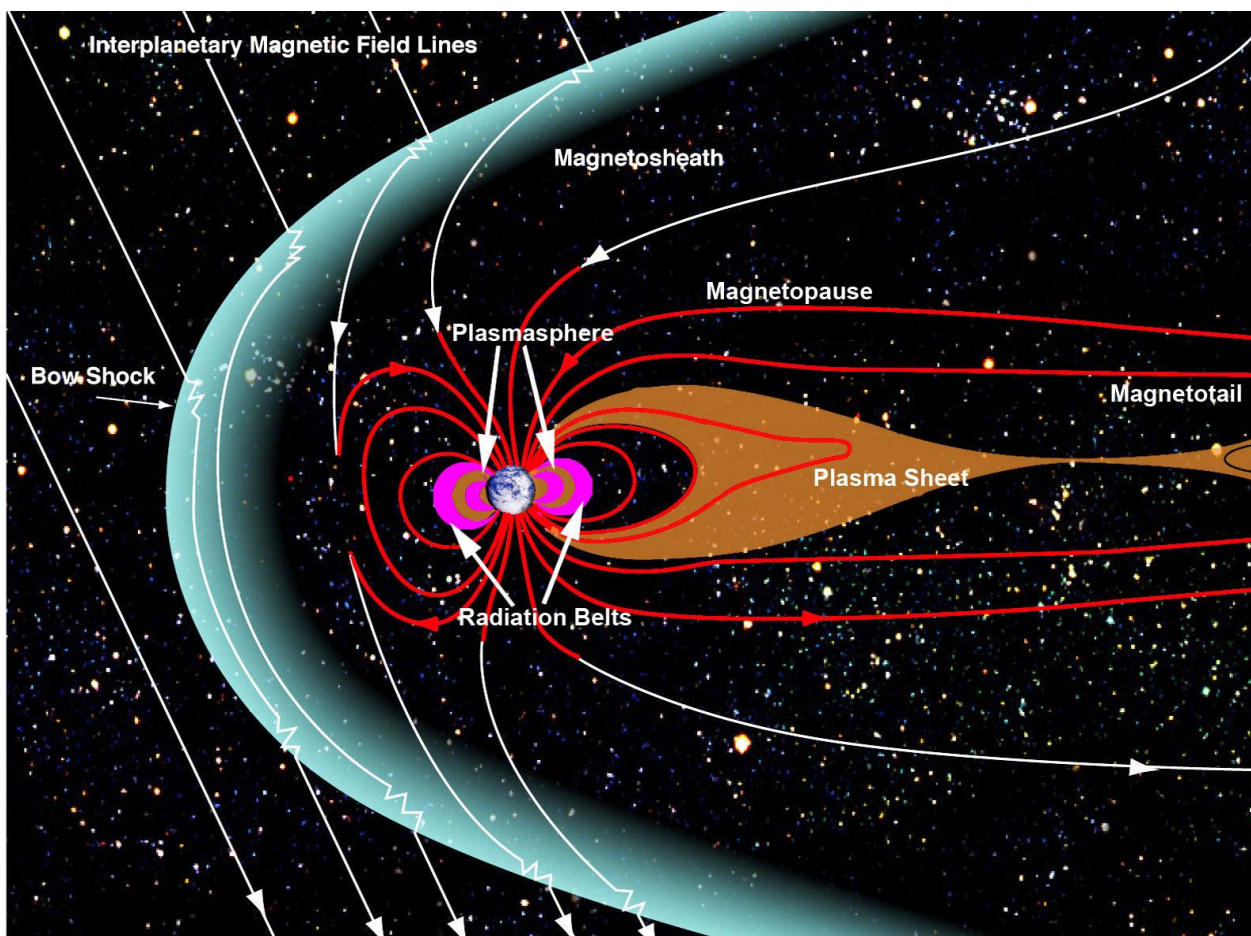


Fig. 1. Structure of the Earth's Magnetosphere¹

1. Earth's magnetosphereⁱⁱ

The Earth's magnetosphere is subdivided into the magnetosheath, magnetopause, magnetotail, plasma sheet, plasmasphere and radiation belts as shown in Fig. 1. These divisions are based on the magnetic field-lines and plasma such as their origins, density and energy level. For example, the magnetopause separates the geomagnetic field and plasma of Earth origin from the interplanetary magnetic field and plasma of Solar origin. Of importance to us in this article are the electrons in the radiation belts. They are of close proximity to Earth, overlap with the geostationary orbit and energetic radiation.

A plasma is a gas of free charged particles that is electrically neutral due to it having similar numbers of positive and negative charges. In the case of low particle densities or high particle kinetic energies relative to the potential set up by neighboring charges, the influence of each particle on each other is minimal and they may be considered independently.

The radiation belt is situated between 2 and 6 Earth's radius R_e ($1 R_e = 6371 \text{ km}$), with typical electron fluxes of 10^0 to $10^8 \text{ cm}^{-2}\text{s}^{-1}$ and energies of 0.1MeV to 5MeV at solar minimum. As can be seen from Fig. 1., the Earth's magnetic field in that region may be modeled as a dipole with a field strength varying between 100 to 1000nT.

Earth's magnetic field

$$\mathbf{B}(\mathbf{x}, \mathbf{y}, \mathbf{z}) = -B_0 R_e^3 (x^2 + y^2 + z^2)^{-5} [3xz, 3yz, 2z^2 - x^2 - y^2] \quad (1a)$$

Earth's magnetic field at the equator

$$B(r) = B_0 R_e^3 r^{-3} \quad (1b)$$

B_0 is the magnetic field strength at the Earth's surface measured at the equator.

Under solar wind conditions, this dipole field is compressed and in addition to that is a convection electric field pointing in the dawn-dusk direction Fig.2.

There are three general schemes to modeling the motion of plasma. The simplest is to consider the plasma as consisting of individual and independent charge carriers interacting with background electric and magnetic fields.

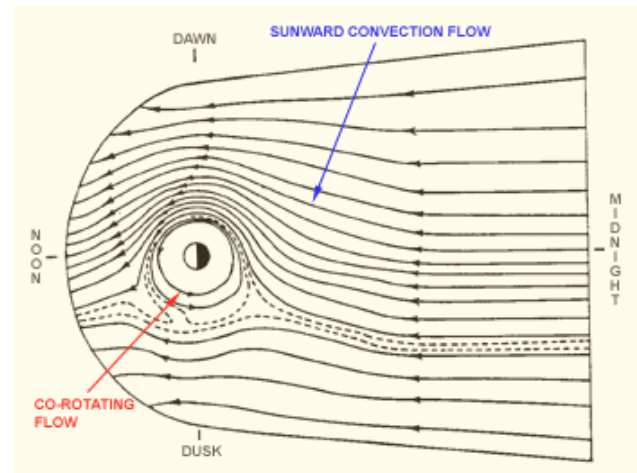


Fig. 2. Earth's Magnetosphere showing plasma trajectories and dawn-dusk directionⁱⁱⁱ

This scheme known as “Single particle motion” or “test particle approximation” neglects the effects of other particles and the effects on the surrounding fields due to the particle in question. This is valid when the test particles have negligible energy density and thus do not affect the background fields in a significant manner. This is a reasonable approximation for radiation belt electrons.

On the other hand, “Magnetohydrodynamics” neglects all single particle aspects and treats the plasma as a single conducting fluid with macroscopic parameters such as density, velocity and temperature. This schemes assumes that the plasma maintains local equilibrium and is thus used to study low-frequency wave phenomena. An extension to multiple fluids to account for different species of particles is possible.

Lastly, the third approach known as “Kinetics” analyses the development of the distribution function for a collection of particles in phase space and is used to model microscopic effects not captured by Magnetohydrodynamics.

2. Relativistic charged-particle motion^{iv}

Single particle motion

This report focuses on “Single Particle Motion” since it is possible to trace the trajectories of charged particles in external fields just based on the Lorentz equation as given below. The effect of the Earth's gravitational field on the motion of these charged particles is neglected.

Relativistic Lorentz equation

$$d(\gamma m \mathbf{v})/dt = q\mathbf{E}(\mathbf{r}) + q\mathbf{v} \times \mathbf{B}(\mathbf{r}) \quad (2a)$$

$$\gamma = (1 - v^2/c^2)^{1/2} \quad (2b)$$

In addition, many explicit integration schemes have been developed to solve the Lorentz equation. Examples are “Leap-frog”, “Runge-Kutta” and “Buneman-Boris”. The details of these integration schemes will be elaborated in the latter half of this section.

Solving the Lorentz equation for charged particles in the Earth's dipole field results in three types of typical particle motions: gyration, bounce and drift as shown in Fig. 3.

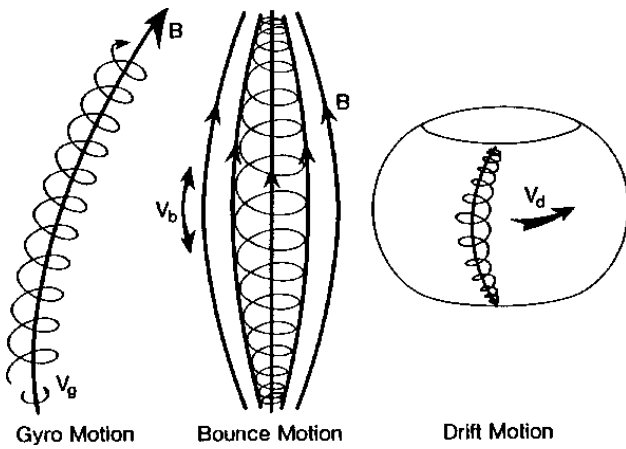


Fig. 3. Typical charged particle motion in the Earth's dipole magnetic field^v

These particle motions can be explained both graphically and mathematically.

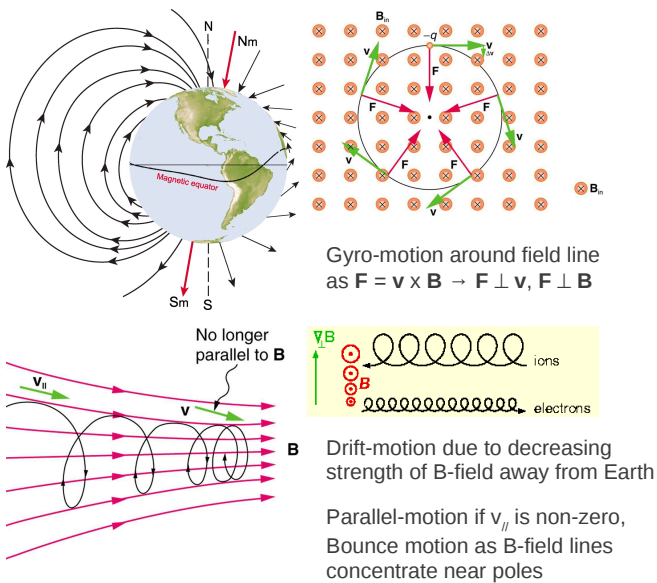


Fig. 4. Properties of Earth's dipole magnetic field and associated particle motions^{vi}.

Fig. 4. Graphically explains the origins of the three particle motion for the case where the Earth's magnetic field resemble that of a simple dipole. On the other hand, mathematically, three motion parameters known as “adiabatic invariants” associated with these three typical particle motions can be defined.

The magnetic moment M is associated with the gyration about magnetic field lines, the longitudinal invariant J is associated with the bounce motion along field lines and the drift invariant Φ is associated with the drift motion around the Earth.

Violation of the invariants, meaning that these parameters no longer remain constant, occur when the time variations of the background fields are faster than the frequency of the associated motions and/or when the spatial variations of background fields are shorter than radius of the associated motions. Changes in the associated motions, characteristics periods, and characteristics radius is synonymous with acceleration and deceleration.

The adiabatic invariants can be obtained via a closed line integral of the canonical momentum for the particle over one cycle of the associated motion. The canonical momentum for a charged particle in a magnetic field with vector potential \mathbf{A} is $\gamma m \mathbf{v} + q\mathbf{A}$.

Using Stokes' theorem,

$$\oint \mathbf{A} \cdot d\mathbf{l} = \int \nabla \times \mathbf{A} \cdot d\mathbf{S} \quad (3)$$

Adiabatic invariants

$$\begin{aligned} J_1 &= \oint_{\text{cyclotron-orbit}} (\gamma m \mathbf{v} + q\mathbf{A}) \cdot d\mathbf{l} \\ &= 2\pi \gamma m \rho v_{\perp} - q \pi \rho^2 B \\ &= (\pi \gamma^2 m^2 v_{\perp}^2) (qB)^{-1} \\ M &= (\gamma^2 m v_{\perp}^2) (2B)^{-1} \end{aligned} \quad (4a)$$

$$\begin{aligned} J_2 &= \oint_{\text{bounce-orbit}} (\gamma m \mathbf{v} + q\mathbf{A}) \cdot d\mathbf{l} \\ &= 2 \int_{\text{mirror-points}} (\gamma m v_{\parallel}) dl \\ &\text{at mirror-point, } M = (\gamma^2 m v_{\perp}^2) (2B)^{-1} = (\gamma^2 m v^2) (2B_m)^{-1} \\ &\text{solving for } v_{\parallel} \text{ using } v_{\perp}^2 = v^2 - v_{\parallel}^2 \\ &= 2 \int_{\text{mirror-points}} (\gamma m v) (1 - B(l)/B_m)^{1/2} dl \\ &= 2\gamma m v J \end{aligned} \quad (4b)$$

$$\begin{aligned} J_3 &= \oint_{\text{drift-orbit}} (\gamma m \mathbf{v} + q\mathbf{A}) \cdot d\mathbf{l} \\ &= \oint_{\text{drift-orbit}} (\gamma m v_d) dl + q \int_{\text{drift-orbit}} (\mathbf{B}) \cdot d\mathbf{S} \\ &\approx q \int_{\text{drift-orbit}} (\mathbf{B}) \cdot d\mathbf{S} = q\Phi \end{aligned} \quad (4c)$$

An approximation exists for particles that conserve the first adiabatic invariant M . In this case, the particle's gyro-frequency is much

faster and gyro-radius is much smaller than the rate at which the background fields are changing. This is known as the “Guiding Center” approximation which treats the motion of the particle as revolving around a moving guiding center as shown in Fig. 5.

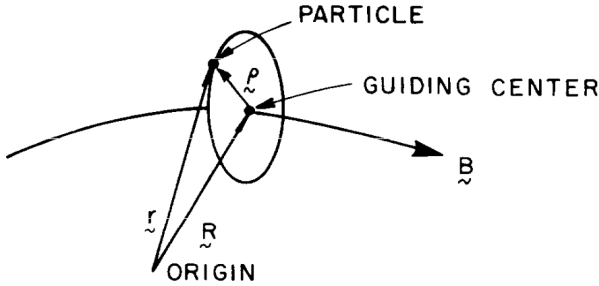


Fig. 5. Gyration about the guiding center^{vii}

In this case, position \mathbf{r} of the particle in the Lorentz equation is replaced by position \mathbf{R} of the guiding center and $\mathbf{r} = \mathbf{R} + \mathbf{p}$. Elimination of higher order terms results in the “Guiding Center” drift equations.^{viii}

Non-relativistic Guiding-Center equations

$$\text{ExB Drift: } \mathbf{v}_E = \mathbf{E} \times \mathbf{B} / B^2 \quad (5a)$$

$$\text{Polarization Drift: } \mathbf{v}_P = (\omega_g B)^{-1} d\mathbf{E}_\perp / dt \quad (5b)$$

$$\text{Gradient Drift: } \mathbf{v}_\nabla = m v_\perp^2 (2qB^3)^{-1} (\mathbf{B} \times \nabla B) \quad (5c)$$

$$\text{Curvature Drift: } \mathbf{v}_R = m v_\perp^2 (qR_c^2 B^2)^{-1} (\mathbf{R}_c \times \mathbf{B}) \quad (5d)$$

Firstly, particle gyration about a guiding center exists so long as a uniform and static magnetic field is present. If the electric or magnetic field is non-static and/or non-homogeneous, drifts occur because the curvature of the particle gyration becomes alternately larger and smaller. The common drift categories are ExB drift, polarization E drift, gradient B drift and curvature B drift.

If the electric field is perpendicular to the magnetic field and static, ExB drift occurs. The properties of this drift does not depend on the properties of the particles. If the electric field is slowly varying in time, polarization drift occurs. If the magnetic field is not uniform, gradient B drift occurs; if field lines are curved, curvature B drift occurs. If the magnetic field is not static, a non-conservative electric field is induced and the energy of the particle changes.

Numerical Integration Schemes

As mentioned earlier, many numerical methods have been developed to solve the Lorentz equation. To name a few are “Leap-frog”, Runge-Kutta” and “Buneman-Boris”.

Linear differential equations

$$d\mathbf{v}/dt = (1/\gamma m)(q\mathbf{E}(\mathbf{r}) + q\mathbf{v} \times \mathbf{B}(\mathbf{r})) \quad (6a)$$

$$d\mathbf{r}/dt = \mathbf{v} \quad (6b)$$

Before looking at the “Leap-frog” method, let us first examine the most simple “Euler” method also known as the “Forward Difference” scheme.

Forward Difference scheme

$$\mathbf{v}_{t+dt} = (1/\gamma m)(q\mathbf{E}(\mathbf{r}_t) + q\mathbf{v}_t \times \mathbf{B}(\mathbf{r}_t))dt + \mathbf{v}_t \quad (7a)$$

$$\mathbf{r}_{t+dt} = \mathbf{v}_t dt + \mathbf{r}_t \quad (7b)$$

By considering $\mathbf{v}_{t+dt} = g\mathbf{v}_t$ and $\mathbf{r}_{t+dt} = g\mathbf{r}_t$, we note that there is no solution g such that $|g| < 1$. As such, the solution is unbounded and unstable. This might be improved by using an average velocity to update the position of the particle.

In “Leap-frog”, the update of position and velocity are interleaved and separated by half a time interval. Although care has to be taken to note the difference in starting time when specifying initial conditions, it is possible to solve for situations where the solution is stable. Furthermore, this is a second order integration scheme meaning that its global error increases as the square of the time interval. As such, its error increases slower than the simpler “Euler” method which is of first order. Similar to the “Euler” method, if an average velocity was used in the velocity update, this method can be further improved as shown in the “Buneman-Boris” scheme later.

Leap-frog method

$$\mathbf{v}_{t+dt/2} = (1/\gamma m)(q\mathbf{E}(\mathbf{r}_t) + q\mathbf{v}_{t-dt/2} \times \mathbf{B}(\mathbf{r}_t))dt + \mathbf{v}_{t-dt/2} \quad (8c)$$

$$\mathbf{r}_{t+dt} = \mathbf{v}_{t-dt/2} dt + \mathbf{r}_t \quad (8d)$$

The simplest “Runge-Kutta” method is the “Euler” method, but it can be extended into higher orders. The idea behind it is a simple division of each full time step into sub time steps and taking the weighted average of the update function from each sub time step to perform the overall update at each full time step.

The most common “Runge-Kutta” method is fourth order.

Implementation of Runge-Kutta4 (9)

Let dy/dt be $f(t,y)$

$$k_1 = f(t,y)$$

$$k_2 = f(t+dt/2, y_t+k_1dt/2)$$

$$k_3 = f(t+dt/2, y_t+k_2dt/2)$$

$$k_4 = f(t+dt, y_t+k_3dt)$$

$$y_{t+dt} = y_t + (dt/6)(k_1+2k_2+2k_3+k_4)$$

$$t = t+dt$$

Finally, the current standard is the “Buneman-Boris” motion solver. Requiring less calculations than the fourth order Runge-Kutta, it is simpler and faster. Similar to the “Leap-frog” method, position and velocity updates are interleaved, velocity update is performed using an averaged velocity. In addition, since the effects of the electric and magnetic field are decoupled during the velocity update, the energy of the particle is exactly conserved in the absence of an electric field. Steps can be taken by the experimenter to transform the frame of reference such that the electric field vanishes.

Buneman-Boris method^{ix} (10)

Update $\mathbf{x}_{i+1/2}$ from $\mathbf{x}_{i-1/2}$ and \mathbf{v}_i

$$\mathbf{x}_{i+1/2} = \mathbf{x}_{i-1/2} + \mathbf{v}_i dt$$

$\mathbf{E}_{i+1/2}$ and $\mathbf{B}_{i+1/2}$ become available

Obtain \mathbf{u}_{i+1} from \mathbf{u}_i and fields $\mathbf{E}_{i+1/2}$, $\mathbf{B}_{i+1/2}$

$$\mathbf{u}_i = \gamma_i \mathbf{v}_i$$

First obtain $\mathbf{u}_{i+1/2}$ from \mathbf{u}_i

$$\mathbf{u}_{i+1/2} = (q/m)(\mathbf{E}_{i+1/2} + (\mathbf{v}_i \times \mathbf{B}_{i+1/2}))(dt/2)$$

Second obtain \mathbf{u}_{i+1} from $\mathbf{u}_{i+1/2}$

$$\mathbf{u}' = \mathbf{u}_{i+1/2} + (q/m)(\mathbf{E}_{i+1/2})(dt/2)$$

$$\boldsymbol{\tau} = (q/m)(\mathbf{B}_{i+1/2})(dt/2)$$

$$\mathbf{u}^* = (1/c)\mathbf{u}'\boldsymbol{\tau}$$

$$\gamma' = (1 + \mathbf{u}'^2/c^2)^{1/2}$$

$$\sigma = \gamma'^2 - \boldsymbol{\tau}^2$$

$$\gamma_{i+1} = ((1/2)(\sigma + (\sigma^2 + 4(\boldsymbol{\tau}^2 + \mathbf{u}'^2)^{1/2}))^{1/2})^{1/2}$$

$$\mathbf{t} = \boldsymbol{\tau}/\gamma_{i+1}$$

$$\mathbf{s} = (1 + \mathbf{t}^2)^{-1}$$

$\mathbf{u}_{i+1} = \mathbf{s}(\mathbf{u}' + (\mathbf{u}' \cdot \mathbf{t})\mathbf{t} + \mathbf{u}' \times \mathbf{t})$

$\mathbf{v}_{i+1} = \gamma_{i+1}^{-1} \mathbf{u}_{i+1}$

Simulation

Particle simulations can be coded using any programming language such as Fortran, C++, Matlab, Mathematica. In this report, Python was used. The Linux commands for installation and execution of Python are given as follows.

Installation: `sudo apt-get install python-numpy python-scipy python-matplotlib ipython ipython-notebook python-pandas python-sympy python-nose`

Execution: `ipython notebook --pylab inline`

The execution command conveniently opens up an iPython browser as shown in Fig. 6.

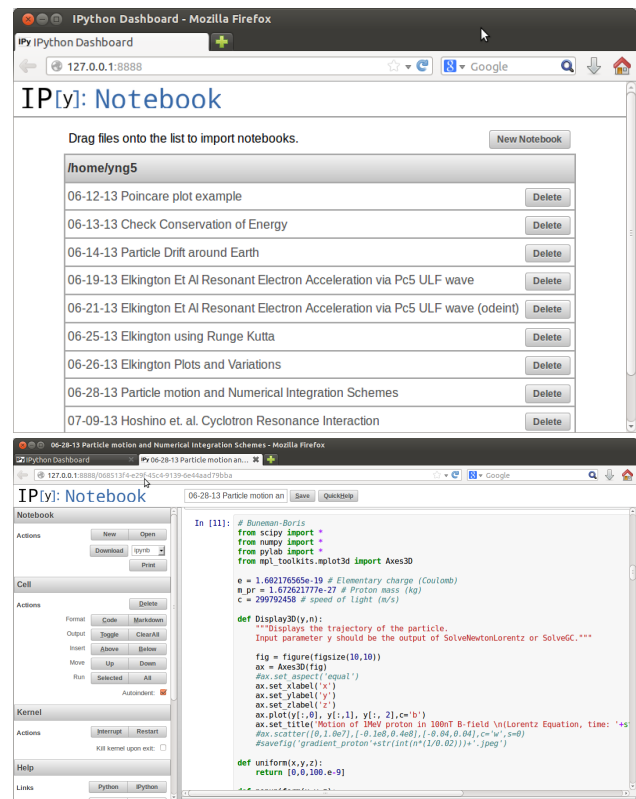


Fig. 6. iPython notebook browser

Some details to note for the simulation of particle motion are the normalization of parameters and plotting of simulation results.

In many particle simulations, normalization of parameters using the characteristic scales of the physical phenomenon was conducted to reduce numerical complexity and also to ease the visualization and understanding results. It is important to check that the equations of motion remain valid after normalization.

Regarding simulation results, two categories exist: instantaneous snapshots and time histories. Examples of quantities recorded for snapshots are particle position and velocity; background field and potential. Examples of quantities recorded for time histories are electrostatic, kinetic and total energies. For the simulation results to be useful in characterizing the physical phenomena, much thought has to be put into selecting descriptive quantities. For example, a phase-space plot would provide much insight into the type of particles that resonantly interact with and are trapped by the background electric and/ or magnetic waves. These plots usually trace the contours of some conserved quantities which may be obtained via solving the equations of motion by hand. As an additional step, the plots obtained manually and via simulation may be cross-checked for correspondence.

3. Summer project

The objective of the summer projects is to explore various methods in which energetic particles may be accelerated towards the Earth where their potential to cause damage greatly increases. Many observations suggest a correlation between periods of high solar winds and increased particle transport. Although there are different theories and models describing the method of transportation such as pitch angle scattering and radial diffusion, this report focuses on the model of resonant acceleration described in the following two papers.

Acceleration of relativistic electrons via resonant interaction with toroidal-mode Pc-5 ULF oscillations - Elkington, S.R., M.K. Hudson, and A.A. Chan 1999.^x

Numerical Study of the Upstream Wave Excitation Mechanism - Hoshino, M., and Terasawa, T. 1985.^{xi}

The first paper describes the drift resonant interaction between relativistic equatorial electrons and global toroidal-mode oscillations which occur as a result of solar activity. Since the resonant frequency is on the order of the drift frequency, the first and second adiabatic invariants are likely to be conserved and guiding center approximations may be applied. The third adiabatic invariant is likely to be violated and

this violation of the third adiabatic invariant may lead to energization of the radiation belt electrons.

The discussion of the second paper describes the cyclotron resonant interaction between charged particles and local circularly-polarized Alfvén waves. Since the resonant frequency is on the order of the cyclotron frequency, the first adiabatic invariant is likely to be violated and acceleration of particles is possible.

Drift resonant interaction

For this simulation, the trajectories of equatorial electrons in a simplified field model was solved. Since the simulation assumes the solar wind scenario, the Earth's magnetic field is that of a compressed dipole, the electric field is a wave superposed on top of an optional dawn-dusk convection field. The electric wave is in the radial direction, as a result of $m=2$ global toroidal mode oscillation of the magnetosphere. It is likely that other mode numbers are present but $m=2$ is studied because it displays resonance at $\omega = \omega_d$. The equations and plots describing the magnetic and electric fields as seen by the particles are given below.

$$B(r, \varphi) = B_0(Re^3/r^3) + b_1(1 + b_2\cos\varphi) \quad (11a)$$

$$E(r, \varphi) = E_0(r, \varphi) + dE_{r2}\sin(m\varphi + \omega t + pE_{r2}) \quad (11b)$$

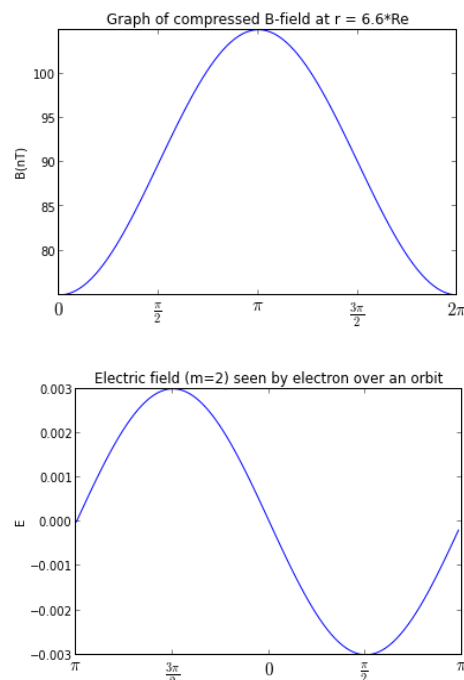


Fig. 7. Magnetic and electric field as seen by an electron over one drift orbit. This shows the magnitudes of the fields used and that the electron is always in phase with the $m=2$ global wave.

Since the particle in question is an electron with a small gyro-radius and high gyro-frequency, the guiding center approximations were employed. Fig. 8. provides a rough guide as to the situations in which the guiding center approximations are appropriate.

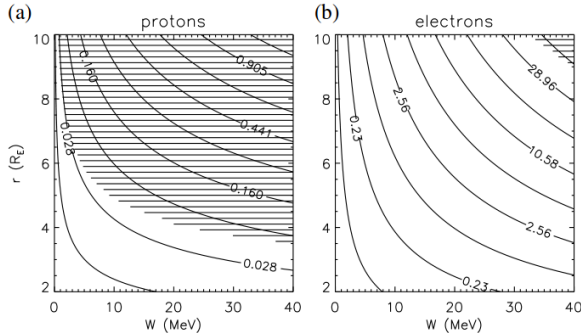


Fig. 8. Lines of constant first adiabatic invariant for protons (a) and electrons (b) in the Earth's dipole field. The unshaded area indicates regions where the guiding-center approximations may be used.^{xiii}

To simplify calculations even further, the magnitude of polarization E drift is usually several orders smaller than ExB drift and is thus safely neglected. Curvature B drift may be ignored if considering only equatorial particles with no bounce motion. As such, only ExB drift and gradient B drift remains to be considered. Thus, the equations of motion used to calculate the trajectory of the equatorial electron are given as follows. Relativistic effects have to be considered because of the high energies of the electrons.

$$dr/dt = E_{\phi}/B - (M/\gamma r B)\delta_{\phi}B \quad (12a)$$

$$d\phi/dt = -E_r/B + (M/\gamma r B)\delta_r B \quad (12b)$$

The following Fig. 9 show the drift trajectories of the electron over one drift period.

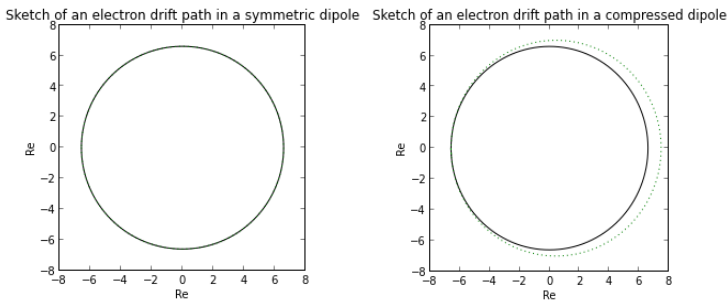


Fig. 9. Drift trajectory for a 1.63MeV electron starting at noon on the left, counterclockwise. Symmetric dipole on the left, compressed dipole on the right. Drift frequency is 2.86mHz and 2.94mHz respectively.

As shown in the previous figures, in the case of a compressed dipole, the particle has a velocity component in the radial direction. Since there is also a component of the electric field in the radial direction, this results in a non-zero $E_r dr$. At the resonant frequency of $\omega = \omega_d = 3\text{mHz}$, the period of the velocity oscillation and the period of the electric field as seen by the electron matches. As such, the radial velocity is always pointing in the opposite direction from the electric field. Consequently, work done by the electric field is non-zero over the entire drift period and the kinetic energy of the electron increases.

The following Fig. 10(a,b,c) shows the work done by the field, the energy gained by the electron and the phase-space trajectory of the same electron over ten drift periods.

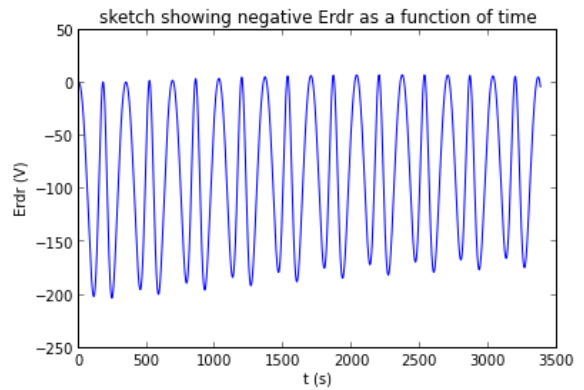


Fig. 10a. Plot showing work done by the electric field over the entire ten drift periods. The integrated $E_r dr$ over the ten drift periods correspond to the same increase in kinetic energy as shown in Fig. 10b.

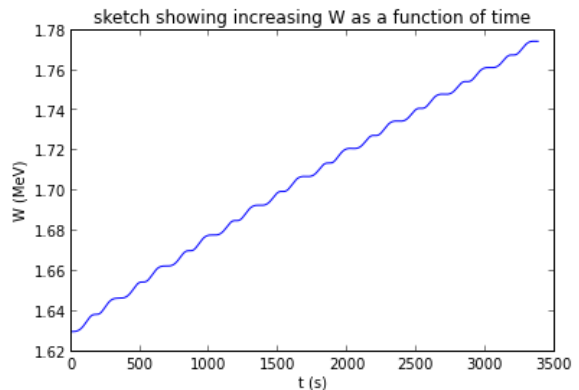


Fig. 10b. Plot showing the increase in kinetic energy of the electron over the entire ten drift periods. This kinetic energy was calculated using the properties of the first adiabatic invariant $M = (\gamma+1)K(2B)^{-1}$.

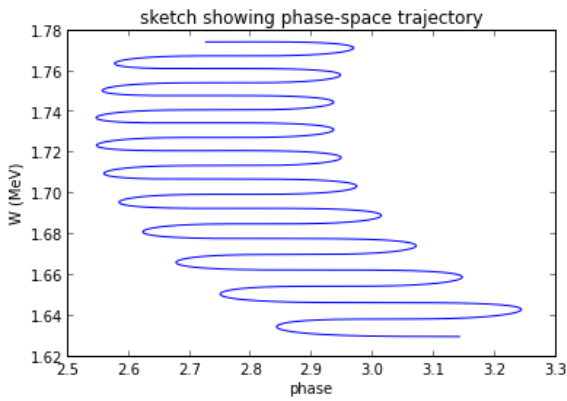


Fig. 10c. Plot showing the phase-space trajectory of the electron over the entire ten drift periods. The electron begins at the bottom right corner and traces the phase-space trajectory upwards. Fig. 11. explains the oscillation in phase for each drift cycle.

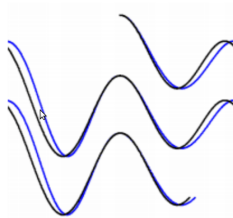
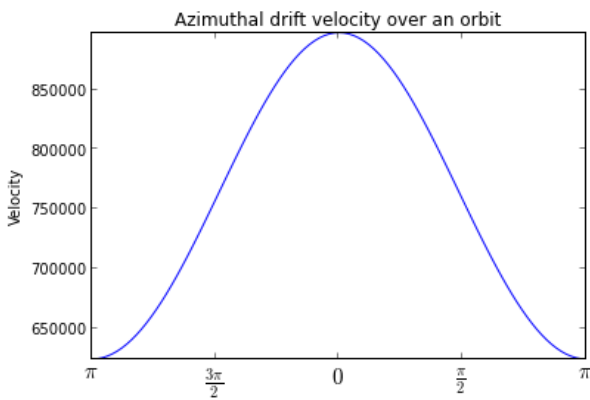


Fig. 11. Plot showing variation in azimuthal velocity over one drift period. On the right, the phase of the wave is shown in blue while that of the particle is shown in black. As the particle gains azimuthal velocity, it advances in phase relative to the wave, the opposite happens when the

particle loses azimuthal velocity. This results in the oscillation in phase-space for each drift cycle that is seen in Fig. 10c.

However, as the electron gains kinetic energy, its velocity and drift frequency increases. Consequently, it falls out of phase from the wave and the reverse resonant interaction occurs, leading to deceleration and a decrease in energy as shown in Fig. 12.

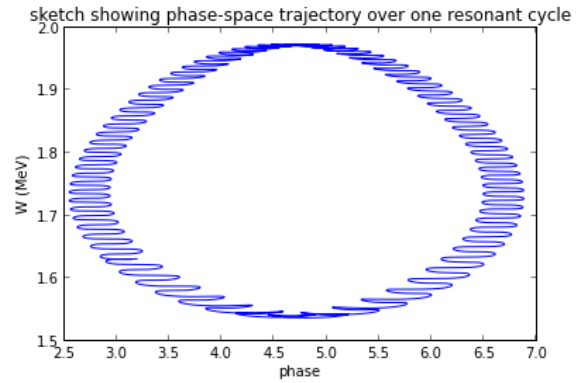
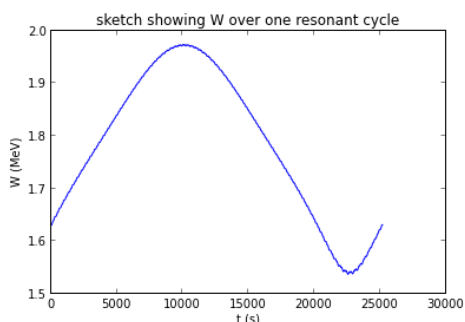


Fig. 12. Plots showing the kinetic energy of the electron over one resonant cycle in time and phase-space. Initially, the kinetic energy of the electron is increasing as shown on the left half of the phase space plot. However, as the electron gains energy and thus speed, it is drifting at a frequency faster than the global $m=2$ wave. As such, it falls out of phase with the wave and the reverse resonant interaction occurs. This traces out an ellipse in the phase space plot. Thus, ellipses in phase space plots are characteristic of resonant interaction.

The same simulations were conducted on electrons with different initial energies and phase to show that this is indeed a resonant interaction. The results are plotted in and Fig. 14.

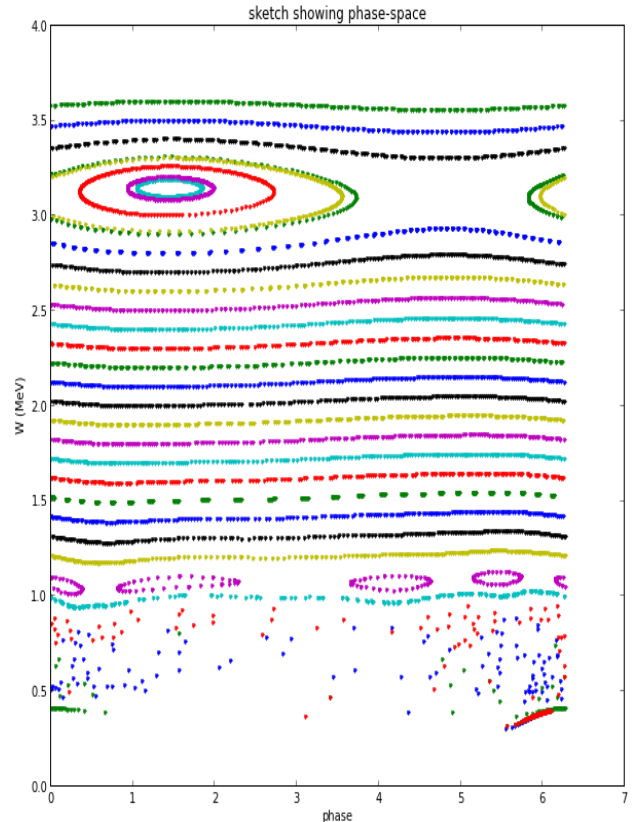


Fig. 13. Phase-space plot showing resonance center at 3.14 MeV and around 1.05 MeV for a 4mHz wave and electrons orbiting at 5.0Re.

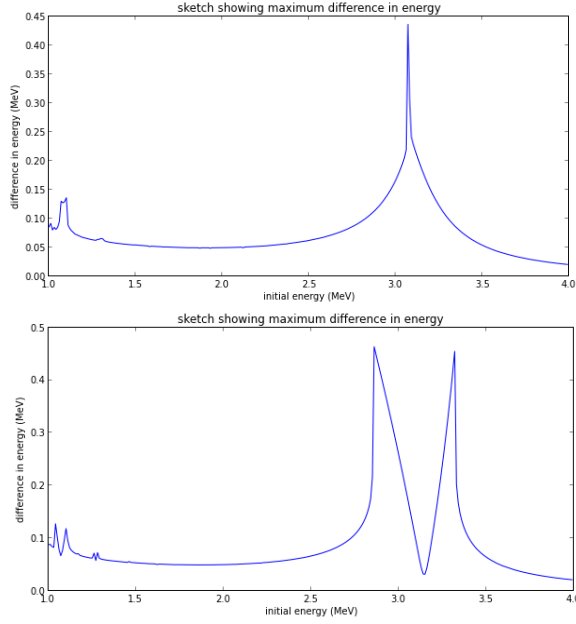


Fig. 14. Plots showing difference in kinetic energies for electrons starting at dawn ($\phi = \pi/2$) and dusk ($\phi = 3\pi/2$). The difference in the plots, peaks at dawn and valleys at dusk, is related to the stable and unstable resonant centers at 3.14MeV and around 1.05MeV.

The resonant condition is $\omega = (m \pm 1)\omega_d$ which corresponds to $\omega_d = \omega/(2 \pm 1) = \omega$ or $\omega/3$ for an $m = 2$ global toroidal mode wave. Solving the following equations for a symmetric dipole field gives resonant kinetic energies of around 3.3MeV and 1.2MeV. However, as shown in Fig. 9., under an asymmetric dipole, drift frequency for an electron of the same kinetic energy is faster and thus the resonant kinetic energy is expected to be lower.

$$\begin{aligned} \gamma &= 1 + Ke/(mc^2) \\ B &= B_0(R_e/r)^3 \\ M &= (\gamma+1)K/B \\ \omega_d &= (3M/(\gamma r))/(2\pi r) \end{aligned}$$

Since Fig. 13. and Fig. 14. shows wave trapping and resonance only at the expected resonant energies, this provides support for acceleration of electrons via resonant interaction. As an additional note, the resonant condition for a global poloidal mode wave is $\omega = m\omega_d$.

The addition of a dawn-dusk convection electric field, realistic in solar wind conditions, shows the possibilities of accelerating particles from energies and phase outside the resonance centers towards the stable resonance center, see Fig. 15.

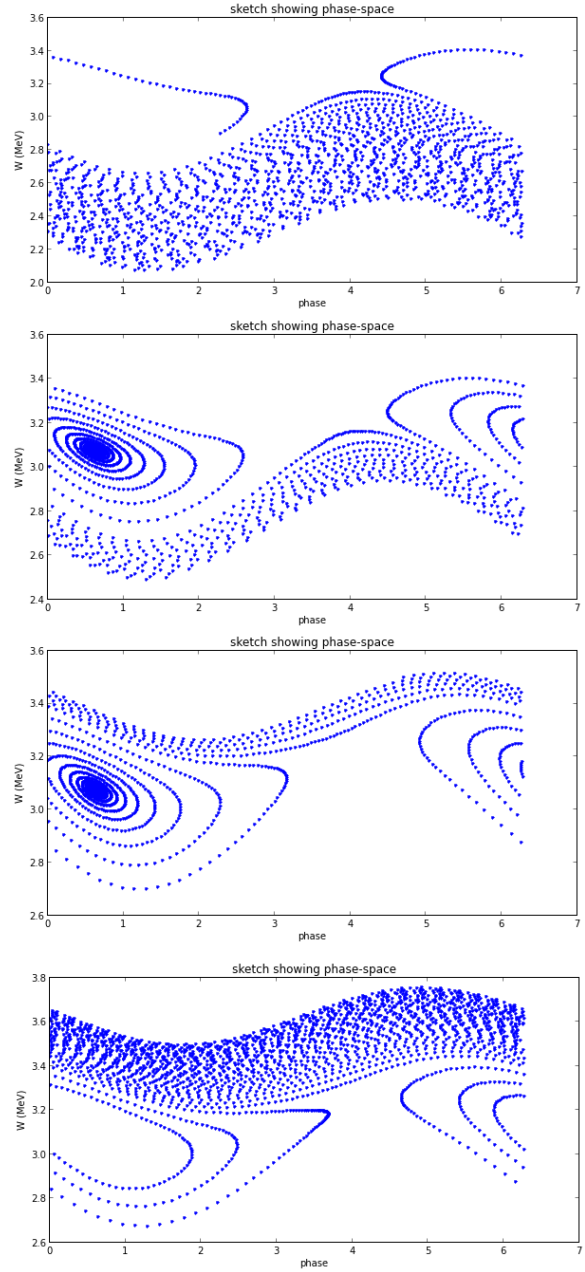


Fig. 15. From top to bottom, 2.5MeV electron starting at two different initial phase condition: dawn and dusk; 3.5MeV electron starting at dawn and dusk. The electrons are shown to have accelerated or decelerated towards the closest resonant center at 3.14MeV.

This might lead to an increase in population of electrons of certain resonant energies during strong solar wind conditions.

In summary, this simulation shows the possibilities of drift resonant acceleration with global $m=2$ toroidal mode waves for electrons where the 1st adiabatic invariant is conserved.

Cyclotron resonant interaction

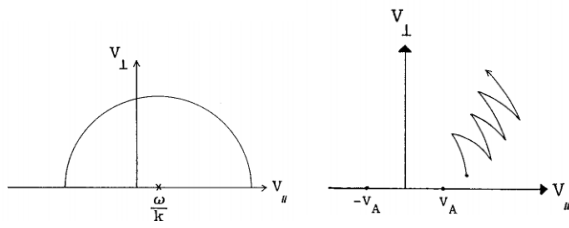


Fig. 16. The figure on the left shows the relationship between V_{\perp} and V_{\parallel} when only a single wave is present. Since the particle traces out a semi-circle with a fixed radius, particle kinetic energy remains constant. The figure on the right shows an increase in particle kinetic energy when both waves traveling in the direction parallel and anti-parallel to the background field are present.^{xiii}

Apart from drift interactions with a low frequency global $m=2$ toroidal mode wave, it is also possible for cyclotron interactions with a higher frequency local circularly polarized Alfvén wave. In the case of multiple waves Fig. 16., scattering by the waves may lead to diffusion in energy and possible particle acceleration. The cyclotron resonant condition as given in “Particle Scattering and Acceleration in a Turbulent Plasma Around Comets” by Terasawa, T. 1989 is shown below.

Resonant condition

$$\omega = k_{\parallel}V_{\parallel} + \Omega_i; V_{\parallel} = (\omega + \Omega_i)/k_{\parallel} \quad (13a)$$

Dispersion relation for Alfvén wave

$$\omega = \pm kV_A \quad (13b)$$

Resonance occurs when

$$k_{\parallel}V_{\parallel} + \Omega_i = \pm kV_A \quad (13c)$$

where V_{\parallel} is the component of the particle's velocity parallel to the background magnetic field and Ω_i is the cyclotron frequency of the particle.

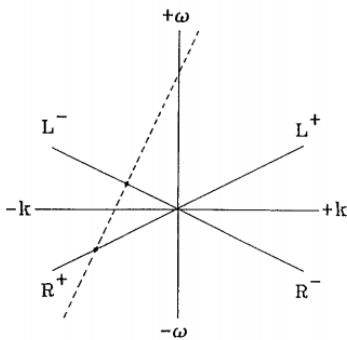


Fig. 17. Dispersion relation of left (L) and right (R) circularly polarized Alfvén waves traveling in the direction parallel (+) and anti-parallel (-) to the background magnetic field and the points where it intersects with the resonant condition.

Equations for the phase-space contours tracing constants of particle motions were derived from the Lorentz equation and expressions of circularly polarized Alfvén waves.

Right circularly polarized, parallel Alfvén wave

$$\omega = \Omega_i/2; V_w = 1; \mathbf{k} = \omega/V_w[1,0,0]; \Omega_w = 0.4 \quad (14)$$

$$\mathbf{B}_w(x,y,z,t) = [0, \Omega_w \cos(\mathbf{k} \cdot \mathbf{x} - \omega t), -\Omega_w \sin(\mathbf{k} \cdot \mathbf{x} - \omega t)] \quad (R+)$$

$$\mathbf{E}_w(x,y,z,t) = (\mathbf{B}_w \times \mathbf{k})V_w$$

Lorentz Equation:

$$\begin{aligned} d(\mathbf{v})/dt &= (q\mathbf{E}(\mathbf{r}) + q\mathbf{v} \times \mathbf{B}(\mathbf{r}))m^{-1} \\ d(\mathbf{r})/dt &= \mathbf{v} \end{aligned} \quad (15a)$$

Lorentz Equation modified to record

v_{\parallel} , v_{\perp} and ϕ_{diff} after inserting wave expression:

$$d(v_{\parallel})/dt = \Omega_w v_{\perp} \sin(\phi_{\text{diff}}) \quad (15b)$$

$$d(v_{\perp})/dt = -\Omega_w (v_{\parallel} - \omega/k) \sin(\phi_{\text{diff}})$$

$$d(\phi_{\text{diff}})/dt = \Omega_w (\omega - kv_{\parallel} \cos(\phi_{\text{diff}})) / (kv_{\perp} - k(v_{\parallel} - V_i))$$

After analytically solving Lorentz equation for constant of motion χ

$$\chi = (1/2)(v_{\parallel} - V_i)^2 - \Omega_w v_{\perp} \cos(\phi_{\text{diff}}) \quad (15c)$$

Fig. 18. shows the phase-space plots for a right-handed Alfvén wave propagating in the same direction as the background magnetic field sketched using various means.

The first plot is obtained through numerically integrating the Lorentz equation modified to record particle velocity and phase difference after substituting wave expression. The definition of phase difference is $\phi_{\text{diff}} = \phi_i - \phi_w$ where ϕ_i is $\tan^{-1}(V_y/V_z) - \phi_w$ is $\tan^{-1}(B_y/B_z)$.

The second plot is obtained mathematically by rearranging for constants of motion – quantities where $d/dt = 0$.

Since both plots are derivatives of the standard Lorentz equation, they should look similar.

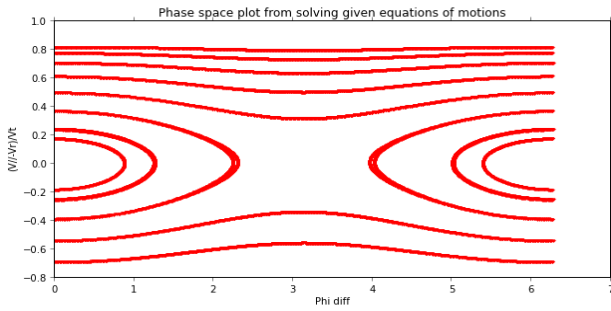


Fig. 18a. Phase-space plot derived numerically from Lorentz equations modified to record particle velocity and phase difference.

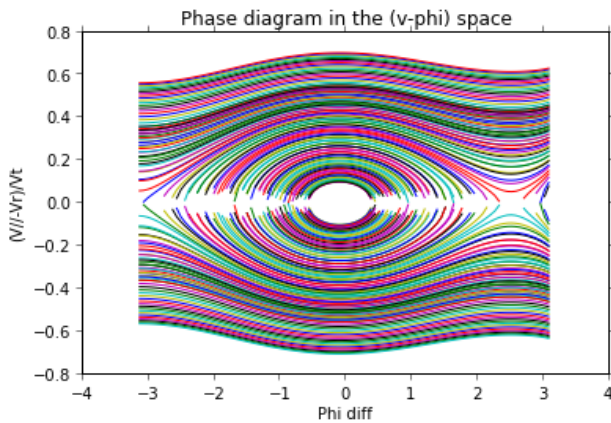


Fig. 18b. Phase-space plots derived analytically through solving for constants of motion from Lorentz equation.

Conclusion

In conclusion, this report presented a quick introduction into the structure of the Earth's magnetosphere, the Lorentz equation and the resulting three typical particle motions. It then provided a simple definition and derivation of the adiabatic invariants. Violation of the adiabatic invariants is synonymous with particle acceleration. Following that, various numerical integration schemes were shown and briefly analyzed. Finally, it focused on reproducing the results of two papers which discussed the possibilities of particle acceleration through drift resonance with global waves and cyclotron resonance with local waves.

Acknowledgements

The author would like to thank the members of Masahiro Hoshino laboratory at the University of Tokyo, Graduate School of Science, Department of Earth and Planetary Science for the guidance, encouragement and many good times spent together. The organizers of UTRIP: University of Tokyo Research Internship Program for the wonderful opportunity.

Scot Elkington for his willingness, prompt and kind assistance in explaining his work in detail.

- i Structure of the Earth's magnetosphere
http://www.nasa.gov/images/content/463951main_magnetosphere2_full.jpg
- ii M. G. Kivelson, C. T. Russell, Introduction to Space Physics, Cambridge University Press, 1995.
- iii Earth's Magnetosphere showing plasma trajectories and dawn-dusk direction
<http://pluto.space.swri.edu/image/glossary/convection2.gif>
- iv W. Baumjohann, R. Treumann, Basic Space Plasma Physics, Imperial College Press, 1997.
D. A. Gurnett, A. Bhattacharjee, Introduction to Plasma Physics: With Space and Laboratory Applications, Cambridge University Press, 2005.
Öztürk, M.K. Trajectories of charged particles trapped in Earth's magnetic field, American Journal of Physics, Volume 80, Issue 5, pp. 420, 2012.
- v Charged particle motion in the Earth's dipole magnetic field
<http://www-ssc.igpp.ucla.edu/ssc/tutorial/msphere07.gif>
- vi Earth's dipole magnetic field
http://www.sciencemag.org/content/336/6084/1054/F1_small.gif
Gyro-motion as a result of homogeneous field lines
http://cnx.org/content/m42375/latest/figure_23_05_02a.jpg
Bounce-motion as field lines become more concentrated
http://cnx.org/content/m42375/latest/figure_23_05_04a.jpg
Drift-motion due to gradient in field strength
<http://www.differ.nl/users/hugodeblank/lectures/zy/Finhomog.gif>
- vii Figure 1 from T. G. Northrop, Adiabatic charged-particle motion, Rev. Geophys., Volume 1, pp. 283, Issue 3, doi:10.1029/RG001i003p00283, 1963.
- viii Northrop, T. G. Adiabatic charged-particle motion, Rev. Geophys., Volume 1, pp. 283, Issue 3, doi:10.1029/RG001i003p00283, 1963.
- ix Vay, J. L. Simulation of beams or plasmas crossing at relativistic velocity Phys. Plasmas 15 056701, 2008.
- x Elkington, S.R., M.K. Hudson, and A.A. Chan, Acceleration of relativistic electrons via resonant interaction with toroidal-mode Pc-5 ULF oscillations, Geophys. Res. Lett., 26(21), 3273, 1999.
Elkington, S.R., M.K. Hudson, M.J. Wiltberger, and J.G. Lyon, MHD/Particle simulations of radiation belt dynamics, J. Atmos. Solar Terr. Phys., 64, 607, 2002.
Elkington, S.R., M.K. Hudson, and A.A. Chan, Resonant acceleration and diffusion of outer zone electrons in an asymmetric geomagnetic field, J. Geophys. Res., 108(A3), 1116, doi:10.1029/2001JA009202, 2003.
Elkington, S.R., M. Wiltberger, A.A. Chan, and D.N. Baker, Physical models of the geospace radiation environment, J. Atmos. Solar Terr. Phys., 66, 1371, doi:10.1016/j.jastp.2004.03.023, 2004.
Elkington, S.R. A review of ULF interactions with radiation belt electrons, in Magnetospheric ULF Waves: Synthesis and New Directions, edited by K. Takahashi, P.J. Chi, R.E. Denton, and R.L. Lysak, AGU Geophysical Monograph 169, AGU, Washington, D.C., 2006.
- xi Hoshino, M., Terasawa, T. Numerical study of the upstream wave excitation mechanism. I. Nonlinear phase bunching of beam ions, J. Geophys. Res., 90(A1), 57–64, 1985.
Terasawa, T. Particle scattering and acceleration in a turbulent plasma around comets, in Plasma waves and instabilities in magnetospheres and at Comets, edited by H. Oya and B. T. Tsurutani, Geophysical Monograph, 53, 41-49, 1989.
- xii Figure 1 from S.R. Elkington et al./Journal of Atmospheric and Solar-Terrestrial Physics 64 (2002) 607–615
- xiii Relationship between V_{\perp} and V_{\parallel} ; dispersion relation of Alfvén wave and intersections with resonant condition
<http://ccdb5fs.kek.jp/cgi-bin/img/allpdf?198804321>